

The Devil is in Temporal Token: High Quality Video Reasoning Segmentation

Sitong Gong¹, Yunzhi Zhuge^{1*}, Lu Zhang¹, Zongxin Yang²,
Pingping Zhang¹, Huchuan Lu¹

¹Dalian University of Technology, ²Havard University

Abstract

Existing methods for Video Reasoning Segmentation rely heavily on a single special token to represent the object in the keyframe or the entire video, inadequately capturing spatial complexity and inter-frame motion. To overcome these challenges, we propose **VRS-HQ**, an end-to-end video reasoning segmentation approach that leverages Multimodal Large Language Models (MLLMs) to inject rich spatiotemporal features into hierarchical tokens. Our key innovations include a Temporal Dynamic Aggregation (TDA) and a Token-driven Keyframe Selection (TKS). Specifically, we design frame-level $\langle \text{SEG} \rangle$ and temporal-level $\langle \text{TAK} \rangle$ tokens that utilize MLLM’s autoregressive learning to effectively capture both local and global information. Subsequently, we apply a similarity-based weighted fusion and frame selection strategy, then utilize SAM2 to perform keyframe segmentation and propagation. To enhance keyframe localization accuracy, the TKS filters keyframes based on SAM2’s occlusion scores during inference. **VRS-HQ** achieves state-of-the-art performance on ReVOS, surpassing VISA by 5.9%/12.5%/9.1% in \mathcal{J} & \mathcal{F} scores across the three subsets. These results highlight the strong temporal reasoning and segmentation capabilities of our method. Code and model weights will be released at [VRS-HQ](#).

1. Introduction

Reasoning segmentation [9, 15, 25, 28, 36], which aims to generate segmentation results from complex query texts, has advanced with multimodal foundation models [16, 19, 27]. However, existing methods [9, 15, 25, 28] focus primarily on image-level segmentation, leaving the more challenging domain of video-level segmentation, which requires temporal reasoning of object relations and attributes, relatively unexplored. To address this gap, Video Reasoning Segmentation (VRS) [1, 37, 42] has recently emerged as a promising approach. Unlike Referring Video Object Segmentation (RVOS) methods [34, 35, 38], which rely on

explicit descriptive phrases like “a person skateboarding”, VRS leverages the extensive world knowledge and temporal reasoning capabilities of Multimodal Large Language Models (MLLMs) to transform implicit intent-based expressions into precise object masklets.

Despite recent advancements in Video Reasoning Segmentation (VRS), such as VISA [37] and VideoLISA [1], significant challenges still exist. **(i) Limited Temporal Context:** Existing methods [1, 37] typically rely on a single segmentation token from an MLLM for keyframe-based segmentation (*cf.* Fig. 1 (a)), resulting in limited temporal context and hindering the effective capture of inter-frame variations and spatiotemporal features. **(ii) Suboptimal Keyframe Detection:** The LLaMA-VID [17] model, used by VISA for keyframe detection, can produce inaccurate keyframes, particularly in videos requiring complex temporal reasoning. **(iii) Decoupled Segmentation and Propagation:** VISA’s reliance on separate, pre-trained models for keyframe segmentation (SAM [14]) and mask propagation (XMem [6]) prevents end-to-end training and inference.

To address the above obstacles, we introduce several strategies to strengthen the VRS model’s proficiency in perceiving spatial information and interpreting temporal dynamics. **Firstly**, current limitations arise from insufficient single-token representation capacity, which restricts the model’s abilities to capture intra-frame spatial features and maintain inter-frame temporal coherence. We hypothesize that encoding frame-level and temporal-level information into hierarchical tokens separately via MLLM and integrating them could effectively unify spatial details with temporal dynamics, enhancing perceptual capability. **Secondly**, the occlusion score introduced by SAM2 [27] inspires us to incorporate the target confidence of each sampled frame as a criterion for keyframe determination. We thus employ the temporal token in conjunction with SAM2 to generate the occlusion scores, applying temporal information for precise keyframe selection. As shown in Fig. 1 (b), our approach locates the cat more accurately compared to VISA, boosting inference efficiency and segmentation performance. **Thirdly**, leveraging SAM2’s integrated seg-

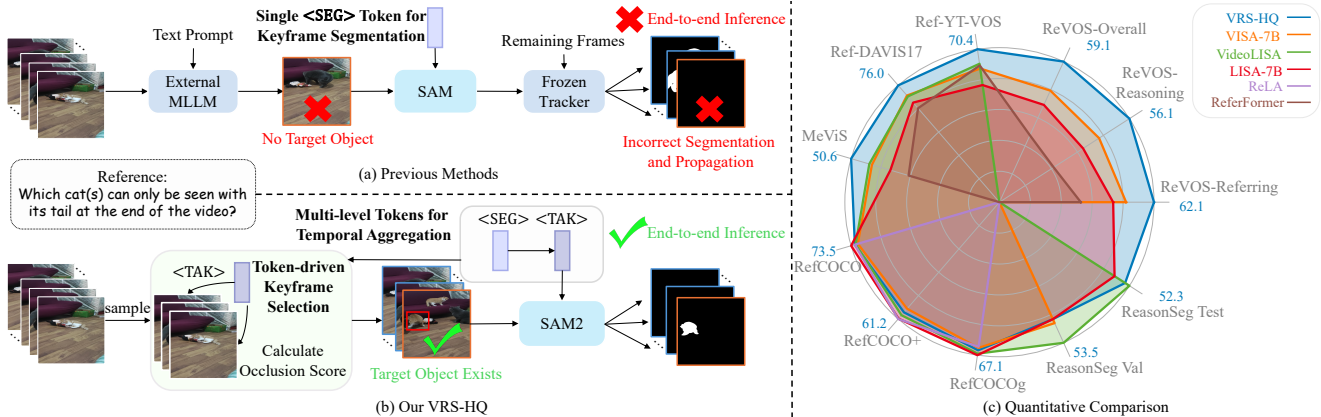


Figure 1. **Comparison with previous VRS approaches.** (a) Previous methods utilize a single $\langle \text{SEG} \rangle$ token for keyframe-based segmentation, depending heavily on external models for keyframe detection and mask propagation. This reliance can hinder accurate keyframe localization and prevent end-to-end inference. (b) In contrast, VRS-HQ introduces frame-level $\langle \text{SEG} \rangle$ and a temporal $\langle \text{TAK} \rangle$ token for dynamic aggregation. The aggregated $\langle \text{TAK} \rangle$ token is then used for both keyframe selection and mask generation within SAM2. This enables single-stage inference with precise keyframe selection and high-quality segmentation. (c) VRS-HQ achieves state-of-the-art performance on various image and video datasets across reasoning and referring segmentation.

mentation and propagation capabilities, we efficiently fine-tune it with our temporal token and its memory mechanism for improved mask quality and inference efficiency.

In this work, we present **VRS-HQ** (High-Quality Video Reasoning Segmentation) (*cf.* Fig. 2), a novel approach that leverages aggregated temporal tokens for enhanced keyframe selection and efficient mask decoding. To begin with, we propose the **Temporal Token Encoding** (§3.1), prompting the MLLM to encode frame- and video-level target features into multi-level special tokens using sampled video frames and tailored conversation templates. The primary innovation lies in the **Temporal Dynamic Aggregation** (§3.2), which employs a cosine similarity-based weighted fusion strategy to merge frame-level $\langle \text{SEG} \rangle$ embeddings into the temporal-level $\langle \text{TAK} \rangle$ embedding, consolidating spatial features into $\langle \text{TAK} \rangle$ while maintaining the temporal consistency of the targets. Subsequently, we select the keyframe according to the token similarity between $\langle \text{SEG} \rangle$ and $\langle \text{TAK} \rangle$ during training. Moreover, we propose the **Token-driven Keyframe Selection** (§3.3) during inference, sequentially treating each sampled frame as a potential keyframe and interacting it with fused $\langle \text{TAK} \rangle$ embedding through SAM2 to calculate an occlusion score. The scores combined with previous token similarity are used as the criterion for keyframe selection. Finally, the keyframe with the fused $\langle \text{TAK} \rangle$ embedding is fed into SAM2 for mask generation, while the remaining frames are treated as non-keyframes and utilize SAM2’s memory mechanism for **Mask Decoding and Propagation** (§3.4).

Through extensive experiments, **VRS-HQ** achieves state-of-the-art performance across a diverse range of video segmentation benchmarks (*cf.* Fig. 1 (c)). Specifically, on the ReVOS [37] dataset, VRS-HQ outperforms VISA-13B by **9.1%** in terms of the $\mathcal{J} \& \mathcal{F}$ metric, highlighting the crit-

ical role of our proposed module in enhancing the reasoning ability for scenes with complex spatiotemporal dynamics. Moreover, VRS-HQ surpasses previous methods by **7.3%/5.6%/6.5%** $\mathcal{J} \& \mathcal{F}$ on three standard referring video segmentation datasets respectively, underscoring its strong inter-frame perception and robust video tracking capabilities. Key contributions can be summarized as follows:

- We present **Temporal Dynamic Aggregation** to blend spatial features from frame-level tokens into a temporal token, endowing the model with the ability to discern inter-frame variations and comprehend the global semantic context of the targets.
- We focus on harnessing the power of temporal tokens in video perception, using the integrated temporal token via SAM2 for keyframe segmentation and propagation. Additionally, we present the **Token-driven Keyframe Selection**, combining each sampled frame with the temporal token to generate occlusion scores via SAM2, providing a reliable basis for keyframe detection.
- By combining the above designs, we introduce **VRS-HQ**, demonstrating state-of-the-art performance on the VRS benchmark and existing RVOS datasets.

2. Related Works

2.1. Referring Video Object Segmentation

Referring Video Object Segmentation [2, 35, 38] (RVOS), which focuses on segmenting and tracking prominent objects in video frames using explicit textual descriptions, has significantly advanced through the integration of visual and linguistic cues. A large proportion of these studies have leveraged attention mechanisms to merge multimodal information. For instance, Wang *et al.* [31] uses asymmetric cross-guided attention to enhance sentence representations

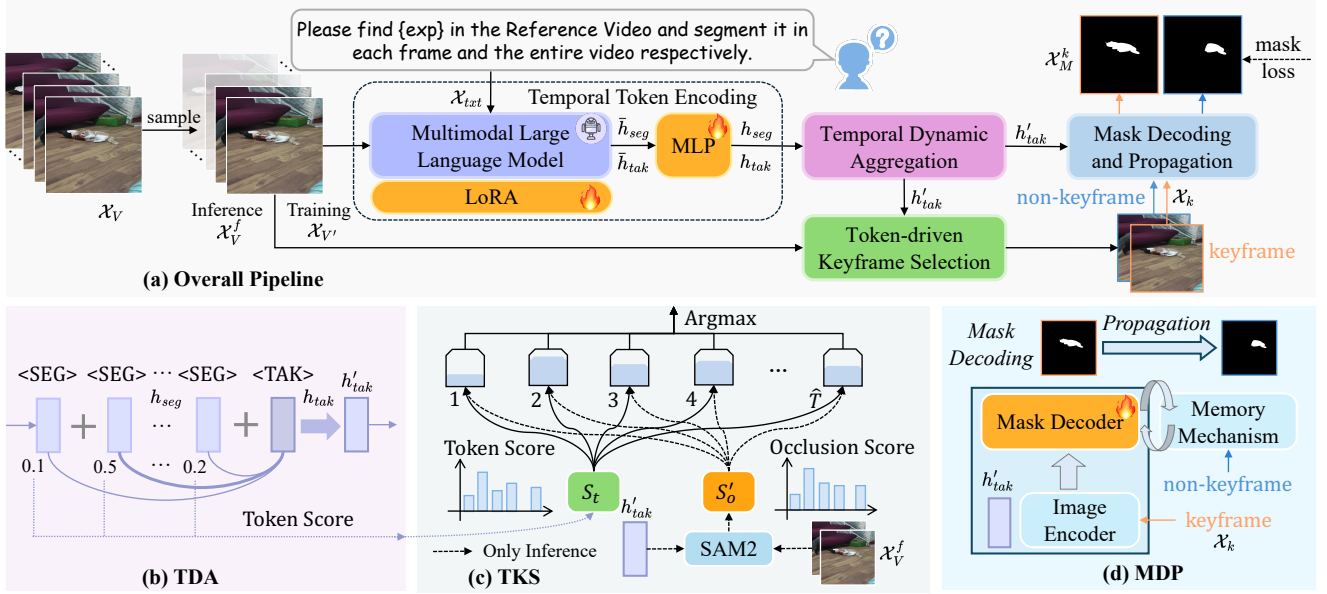


Figure 2. (a) **VRS-HQ architecture**. VRS-HQ incorporates a Multimodal Large Language Model for **Temporal Token Encoding** (<SEG> and <TAK> tokens, §3.1), a Temporal Dynamic Aggregation, a Token-driven Keyframe Selection and Mask Decoding and Propagation. (b) **Temporal Dynamic Aggregation (TDA)** merges frame-level <SEG> tokens into a temporal <TAK> token using a weighted fusion based on cosine similarity. (§3.2). (c) **Token-driven Keyframe Selection (TKS)**. During training, the frame with the <SEG> token closest to the <TAK> token is selected as the keyframe. During inference, keyframe selection is refined using SAM2’s occlusion scores and token similarity scores (§3.3). (d) **Mask Decoding and Propagation (MDP)**. The <TAK> token provides a sparse embedding for SAM2, generating a keyframe mask and propagating it to other frames via a memory mechanism (§3.4).

and aggregate visual context. Seo *et al.* [30] employ cross-modal and memory attention to jointly address RVOS and semi-supervised video object segmentation. Hui *et al.* [11] dynamically recombine linguistic features and interact with visual features using cross-modal attention to highlight spatiotemporal regions of interest. Inspired by DETR [4], methods like MTTR [2] and ReferFormer [35] leverage language queries for precise target localization. While RVOS excels with explicit object descriptions, it often struggles with the complex reasoning required to interpret more implicit and intricate language instructions, motivating our exploration of Video Reasoning Segmentation.

2.2. Reasoning Segmentation

Reasoning segmentation [15, 25, 28, 36] advances referring segmentation by generating masks from complex images and versatile text prompts. LISA [15] pioneers the field of reasoning segmentation. It introduces a new token to expand the vocabulary and proposes the embedding-as-mask paradigm, enhancing segmentation capabilities to address scenarios requiring complex reasoning and world knowledge. LISA++ [40] addresses LISA’s limitations in distinguishing individual instances by enhancing instruction-tuning data with key segmentation datasets, supporting both semantic and instance segmentation tasks. PixelLM [28] innovatively combines a novel pixel decoder and a segmentation codebook with learnable tokens to efficiently gener-

ate high-quality masks without external models. VISA [37] introduces reasoning segmentation to the video domain, proposing reasoning video object segmentation. It uses a pre-trained Multimodal Large Language Model (MLLM) to select keyframes, segments them based on reasoning, and propagates the masks to other frames using a pre-trained object tracker. However, it suffers from limited representation capability of a single special token, inaccurate keyframe selection, and the inability to perform end-to-end inference, compromising its segmentation and tracking performance.

3. Methodology

Task Definition. The task of Video Reasoning Segmentation can be briefly outlined as follows. Given a video clip consisting of T frames $\mathcal{X}_V \in \mathbb{R}^{T \times 3 \times H \times W}$, where H and W denote the height and width of each frame respectively, along with a high-level textual instruction \mathcal{X}_{txt} , VRS aims to design a model \mathcal{M} to interpret and transform \mathcal{X}_{txt} into the binary segmentation mask sequence $\mathcal{X}_M \in \mathbb{R}^{T \times H \times W}$ for each frame. In contrast to RVOS tasks providing explicit descriptions like “the person skateboarding,” VRS typically employs expressions incorporating world knowledge like “tool(s) for holding garbage” or temporal logic like “the ship(s) moving at the highest speed.,” raising higher demands on the model’s capabilities of temporal relationship comprehension and complex scenario reasoning.

Overall Architecture. Fig. 2 illustrates the VRS-HQ architecture, which comprises Chat-UniVi [12] as the Multimodal Large Language Model (MLLM) for temporal token encoding (§3.1), a Temporal Dynamic Aggregation (§3.2), a Token-driven Keyframe Selection (§3.3), and Mask Decoding and Propagation (§3.4). The MLLM encodes the textual prompt into multi-level tokens representing spatial and semantic target information. These tokens drive both temporal dynamic aggregation and keyframe selection via cosine similarity scores. SAM2 then segments the keyframes and tracks the target object throughout the video. During inference, the Token-driven Keyframe Selection computes object occlusion scores for each sampled frame by merging it with the fused temporal token. Filtering keyframes based on these scores improves the accurate localization of the target object and subsequently segmentation process.

3.1. Temporal Token Encoding

Current VRS approaches [1, 37] typically use specified language prompts to guide MLLMs in embedding target information from keyframes or entire videos into a single specialized token, struggling to capture rich spatiotemporal dynamics essential for fine-grained video understanding. To equip the MLLM with both frame-level and video-level contextual awareness for video segmentation, we propose encoding intra-frame spatial information and inter-frame temporal relations into hierarchical tokens.

Hierarchical Token Generation. Instead of previous single-token encoding strategy, the vocabulary of the MLLM is initially augmented with two new special tokens: <SEG> and <TAK>. Then, we design a structured conversational template as “**USER:** Please find {expression} in the Reference Video and segment it in each frame and the entire video respectively.” Here, “{expression}” denotes the target object description. The tokenized prompts \mathcal{X}_{txt} and sampled video frames $\mathcal{X}_{V'}$ are input into the MLLM, which generates a response y_{txt} containing multiple frame-level <SEG> tokens and a temporal-level <TAK> token through autoregressive encoding.

Token Extraction and Mapping. Subsequently, the <SEG> token embeddings $\bar{h}_{seg} \in \mathbb{R}^{T' \times d'}$ and the <TAK> token embedding $\bar{h}_{tak} \in \mathbb{R}^{1 \times d'}$ are extracted from the MLLM’s final layer, where d' denotes the MLLM’s embedding dimension and T' denotes the length of sampled frames. These embeddings are then projected into the same feature space as SAM2 using a multi-layer perceptron:

$$h_{seg}, h_{tak} = MLP(\bar{h}_{seg}), MLP(\bar{h}_{tak}) \quad (1)$$

Here, $h_{seg} \in \mathbb{R}^{T' \times d}$ and $h_{tak} \in \mathbb{R}^{1 \times d}$ represent the sparse embeddings for segmentation mask activation, and d denotes the feature dimension of SAM2. Finally, the frame-

level embeddings h_{seg} are aggregated with the video-level embedding h_{tak} to incorporate temporal dynamics.

3.2. Temporal Dynamic Aggregation

Building on the strong temporal encoding of MLLM, <SEG> and <TAK> embeddings encapsulate the spatial priors and temporal semantic signals of the targets respectively, providing rich contextual information for the segmentation model. Accordingly, we propose the Temporal Dynamic Aggregation to facilitate the fusion of positional and semantic information of the targets.

Keyframes as Token Similarity. The cosine similarity between each frame-level <SEG> token and the temporal-level <TAK> token reflects the semantic alignment between individual frames and the overall video context. We hypothesize that high-similarity frames are more representative of the video’s content and thus suitable as keyframes. This motivates our use of token similarity for keyframe selection during training, which also facilitates weighted fusion of <SEG> and <TAK> tokens.

Similarity-based Weighted Fusion. To enhance the inter-frame consistency while achieving more precise discernment of the object’s positional shifts across frames, we fuse the frame-level embeddings h_{seg} with the video-level embedding h_{tak} using normalized cosine similarity scores as attention weights (*cf.* Fig. 2 (b)). During backpropagation, frame-level features h_{seg} are updated alongside the temporal-level embedding h_{tak} to enable more comprehensive learning of local and global video context:

$$h'_{tak} = h_{tak} + \alpha \sum_{i=1}^{T'} \lambda_i h_{seg}[i], \quad (2)$$

where λ_i represents the normalized cosine similarity between $h_{seg}[i]$ and h_{tak} , and α is the fusion coefficient. The resulting fused embedding h'_{tak} is then used for keyframe selection during inference and mask generation.

3.3. Token-driven Keyframe Selection

VISA [37] relies on an external model (LLaMA-VID [17]) for keyframe selection during inference, hindering end-to-end processing and potentially degrading performance due to inaccuracies in the external model’s output. To address this limitation, we introduce the Token-driven Keyframe Selection that leverages the temporal information encoded within the integrated <TAK> embedding. This approach eliminates the need for complex prompt engineering and significantly improves the reliability of keyframe selection.

Instead of uniform video sampling during training, we adopt the CLIP model [23] to find the frame most aligned with the expression \mathcal{X}_{exp} for inference. The anchor frame is used for global sampling, resulting in sampled frames

$\mathcal{X}_V^f \in \mathbb{R}^{\hat{T} \times 3 \times H \times W}$, where \hat{T} represents the number of the sampled frames. Following the temporal dynamic aggregation (Eq. 2), each sampled frame is treated as a potential keyframe, along with the fused <TAK> embedding h'_{tak} , is sent to SAM2 to generate the object occlusion scores $S_o \in \mathbb{R}^{\hat{T} \times 1}$ (cf. Fig. 2 (c)):

$$S_o = \mathcal{MD}(\mathcal{E}(\mathcal{X}_V^f), h'_{tak}) \quad (3)$$

The occlusion scores effectively indicate the confidence of the target’s presence in the current frame, assisting in identifying which frame best corresponds to the information encoded in the <TAK> token. After determining the keyframe index by the combination of softmax-normalized scores S'_o with token similarity scores S_t , we decode the keyframe mask and then utilize the cross-frame propagation technique of SAM2 to obtain video-level segmentation masks.

3.4. Mask Decoding and Propagation

Following temporal token fusion and keyframe selection, the mask embeddings enriched with positional and semantic information can be yielded by the segmentation model. In contrast to prior methods [1, 37, 42] depending on image-level segmentation models or external object trackers for target trajectories prediction, we utilize SAM2 to perform segmentation and propagation concurrently.

SAM2 for Masklets Decoding. Given the keyframe \mathcal{X}_k , we first extract its features using the image encoder \mathcal{E} , providing the conditional input for SAM2. The integrated temporal embedding h'_{tak} then interacts with these keyframe features within the mask decoder \mathcal{MD} (cf. Fig. 2 (d)) to generate the keyframe mask:

$$\mathcal{X}_M^k = \mathcal{MD}(\mathcal{E}(\mathcal{X}_k), h'_{tak}), \quad (4)$$

where \mathcal{X}_M^k represents the predicted mask for the keyframe. Next, we propagate this mask to two adjacent frames, \mathcal{X}_{k-1} and \mathcal{X}_{k+1} , treated as non-conditional frames, using the memory storage and interaction mechanism. This yields the mask sequence \mathcal{X}_M^s . During inference, all remaining frames are processed as non-conditional frames, facilitating mask propagation throughout the entire video.

3.5. Training Objectives

Our method is trained end-to-end using a combined text generation loss and mask loss to optimize the <TAK> and <SEG> embeddings. The mask loss combines binary cross-entropy (BCE) and DICE loss:

$$L_{total} = \lambda_{txt} L_{txt}(y_{txt}, \hat{y}_{txt}) + \lambda_{mask} L_{mask}, \quad (5)$$

$$L_{mask} = \lambda_{bce} L_{bce}(\mathcal{X}_M^s, \hat{\mathcal{X}}_M^s) + \lambda_{dice} L_{dice}(\mathcal{X}_M^s, \hat{\mathcal{X}}_M^s), \quad (6)$$

where \hat{y}_{txt} and $\hat{\mathcal{X}}_M^s$ represent the ground truth text and mask, respectively, and y_{txt} and \mathcal{X}_M^s are their corresponding predictions. The weighting coefficients λ_{txt} , λ_{mask} , λ_{bce} , and λ_{dice} are set to 1, 1, 2 and 0.5, respectively.

4. Experiments

4.1. Datasets and Metrics

Datasets. Our model is trained and evaluated on extensive image and video segmentation datasets, LLaVA-Instruct-150k [19], as well as the Video Question-Answering datasets from Video-ChatGPT [20]. Specifically, the image segmentation datasets comprise semantic segmentation: ADE20K [44], COCO-Stuff [3], PACO-LVIS [24], and PASCALPart [5], referring segmentation: refCLEF, refCOCO, refCOCO+ [13], and refCOCog [21], and reasoning segmentation: ReasonSeg [15]. While the video segmentation datasets encompass the RVOS datasets: Ref-Youtube-VOS [30], Ref-DAVIS17 [22] and MeViS [7], and the VRS benchmark ReVOS [37].

Evaluation Metrics. We evaluate video segmentation using region similarity (\mathcal{J}), contour accuracy (\mathcal{F}), and their mean ($\mathcal{J}\&\mathcal{F}$). Image segmentation accuracy is measured via Generalized Intersection over Union (gIoU) [29] and Complete Intersection over Union (cIoU) [43]. Model hallucination is assessed using the robustness score \mathcal{R} [37].

4.2. Implementation Details

We fine-tuned Chat-UniVi [12] (our chosen MLLM) using LoRA [10] (rank 8), optimizing the mask decoder and MLP projection layer while freezing other parameters. Training used AdamW (learning rate 0.0003, no weight decay) with a WarmupDecayLR scheduler (100-iteration warmup). We set the fusion coefficient α to 0.1 and sampled two non-keyframes per video. Trained for 7500 iterations on a hybrid image/video dataset using four A800 GPUs with DeepSpeed [26] (batch size 1, gradient accumulation 32, total batch size 128), the model employed TDA for video data (token fusion, segmentation, and propagation) and the <TAK> token for direct segmentation on image data.

4.3. Comparison Results

To showcase the robust pixel-level perception and generalization of VRS-HQ, we conduct evaluations across diverse benchmarks, including ReVOS, RVOS, and image-based referring and reasoning segmentation datasets.

ReVOS Datasets. Tab. 1 illustrates the performance comparison with previous methods [2, 15, 35, 37, 45] on the ReVOS benchmark. VRS-HQ demonstrates significant improvements over the previous state-of-the-art, VISA [37] across all ten metrics. Remarkably, in terms of the $\mathcal{J}\&\mathcal{F}$,

Table 1. Performance comparison with previous methods on ReVOS dataset.

Methods	Backbone	referring			reasoning			overall			\mathcal{R}
		\mathcal{J}	\mathcal{F}	$\mathcal{J}\&\mathcal{F}$	\mathcal{J}	\mathcal{F}	$\mathcal{J}\&\mathcal{F}$	\mathcal{J}	\mathcal{F}	$\mathcal{J}\&\mathcal{F}$	
MTTR [2] <small>[CVPR2022]</small>	Video-Swin-T	29.8	30.2	30.0	20.4	21.5	21.0	25.1	25.9	25.5	5.6
LMPM [7] <small>[ICCV2023]</small>	Swin-T	29.0	39.1	34.1	13.3	24.3	18.8	21.2	31.7	26.4	3.2
ReferFormer [35] <small>[CVPR2022]</small>	Video-Swin-B	31.2	34.3	32.7	21.3	25.6	23.4	26.2	29.9	28.1	8.8
LISA [15] <small>[CVPR2024]</small>	LLaVA-7B	44.3	47.1	45.7	33.8	38.4	36.1	39.1	42.7	40.9	9.3
LISA [15] <small>[CVPR2024]</small>	LLaVA-13B	45.2	47.9	46.6	34.3	39.1	36.7	39.8	43.5	41.6	8.6
TrackGPT [45] <small>[arXiv2023]</small>	LLaVA-7B	46.7	49.7	48.2	36.8	41.2	39.0	41.8	45.5	43.6	11.6
TrackGPT [45] <small>[arXiv2023]</small>	LLaVA-13B	48.3	50.6	49.5	38.1	42.9	40.5	43.2	46.8	45.0	12.8
VISA [37] <small>[ECCV2024]</small>	LLaVA-7B	49.4	52.6	51.0	40.5	45.8	43.2	44.9	49.2	47.1	15.3
VISA [37] <small>[ECCV2024]</small>	LLaVA-13B	55.7	59.0	57.4	41.9	46.5	44.2	48.8	52.8	50.8	15.1
VISA [37] <small>[ECCV2024]</small>	Chat-UniVi-7B	49.2	52.6	50.9	40.6	45.4	43.0	44.9	49.0	46.9	15.5
VISA [37] <small>[ECCV2024]</small>	Chat-UniVi-13B	55.6	59.1	57.4	42.0	46.7	44.3	48.8	52.9	50.9	14.5
VRS-HQ <small>[Ours]</small>	Chat-UniVi-7B	<u>59.8</u>	<u>64.5</u>	<u>62.1</u>	<u>53.5</u>	<u>58.7</u>	<u>56.1</u>	<u>56.6</u>	<u>61.6</u>	<u>59.1</u>	19.7
VRS-HQ <small>[Ours]</small>	Chat-UniVi-13B	61.1	65.5	63.3	54.1	59.4	56.8	57.6	62.5	60.0	<u>18.9</u>

Table 2. Performance comparison with previous methods on the validation sets of RVOS datasets.

Methods	Backbone	Ref-YouTube-VOS			Ref-DAVIS17			MeViS		
		\mathcal{J}	\mathcal{F}	$\mathcal{J}\&\mathcal{F}$	\mathcal{J}	\mathcal{F}	$\mathcal{J}\&\mathcal{F}$	\mathcal{J}	\mathcal{F}	$\mathcal{J}\&\mathcal{F}$
MTTR [2] <small>[CVPR2022]</small>	Video-Swin-T	54.0	56.6	55.3	-	-	-	28.8	31.2	30.0
LMPM [7] <small>[ICCV2023]</small>	Swin-T	-	-	-	-	-	-	34.2	40.2	37.2
ReferFormer [35] <small>[CVPR2022]</small>	Video-Swin-B	61.3	64.6	62.9	58.1	64.1	61.1	29.8	32.2	31.0
OnlineRefer [34] <small>[CVPR2023]</small>	Swin-L	61.6	65.5	63.5	61.6	67.7	64.8	-	-	-
LISA [15] <small>[CVPR2024]</small>	LLaVA-7B	53.4	54.3	53.9	62.2	67.3	64.8	35.1	39.4	37.2
LISA [15] <small>[CVPR2024]</small>	LLaVA-13B	54.0	54.8	54.4	63.2	68.8	66.0	35.8	40.0	37.9
TrackGPT [45] <small>[arXiv2023]</small>	LLaVA-7B	55.3	57.4	56.4	59.4	67.0	63.2	37.6	42.6	40.1
TrackGPT [45] <small>[arXiv2023]</small>	LLaVA-13B	58.1	60.8	59.5	62.7	70.4	66.5	39.2	43.1	41.2
VISA [37] <small>[ECCV2024]</small>	Chat-UniVi-7B	59.8	63.2	61.5	66.3	72.5	69.4	40.7	46.3	43.5
VISA [37] <small>[ECCV2024]</small>	Chat-UniVi-13B	61.4	64.7	63.0	67.0	73.8	70.4	41.8	47.1	44.5
VideoLISA [1] <small>[NeurIPS2024]</small>	LLaVA-Phi-3-V	61.7	65.7	63.7	64.9	72.7	68.8	41.3	47.6	44.4
VRS-HQ <small>[Ours]</small>	Chat-UniVi-7B	<u>68.3</u>	<u>72.5</u>	<u>70.4</u>	72.6	79.4	76.0	<u>47.6</u>	53.7	<u>50.6</u>
VRS-HQ <small>[Ours]</small>	Chat-UniVi-13B	69.0	73.1	71.0	<u>71.0</u>	<u>77.9</u>	<u>74.4</u>	48.0	53.7	50.9

VRS-HQ-13B surpasses VISA-13B by **5.9%** on the referring subset and **12.5%** on the reasoning subset, respectively. These gains highlight the effectiveness of our temporal aggregation strategy and the utilization of the $\langle \text{TAK} \rangle$ token for keyframe selection and target segmentation, which enhances the model’s reasoning capabilities. In contrast, VISA relies on LLaMA-VID [17] for keyframe selection during inference. This strategy may neglect intra-frame fine-grained visual details, leading to inaccurate keyframe localization. Furthermore, the robustness score \mathcal{R} exceeds VISA-13B by **4.4%**, indicating VRS-HQ’s superior capability in handling negative samples.

RVOS. Tab. 2 compares VRS-HQ with state-of-the-art RVOS methods. On Ref-YouTube-VOS and Ref-DAVIS17, VRS-HQ-13B surpasses VideoLISA [1] and VISA-13B [37], achieving $\mathcal{J}\&\mathcal{F}$ improvements of **7.3%** and **5.6%**, respectively. Furthermore, on the motion-intensive MeViS dataset, VRS-HQ-13B yields substantial gains of **6.2%**, **6.1%** and **6.4%** in \mathcal{J} , \mathcal{F} and $\mathcal{J}\&\mathcal{F}$, respectively, demonstrating its effective in capturing mo-

tion and maintaining temporal coherence. These improvements, compared to VideoLISA’s single-token representation, are attributed to the enhanced inter-frame perception of the TDA and the refined keyframe localization of the TKS.

RIS. Our method seamlessly extends to referring image segmentation (RIS) by treating images as single-frame videos. As shown in Tab. 3, VRS-HQ consistently outperforms VISA on three RIS benchmarks, achieving performance comparable to LISA [15] and VideoLISA [1]. On ReasonSeg, VRS-HQ performs competitively, ranking merely below VideoLISA, demonstrating strong generalization. The marginally lower performance on image datasets compared to video datasets likely stems from two factors: (i) our model’s training emphasis on video data (unlike LISA, which is pre-trained solely on images); and (ii) our training methodology encourages reliance on SAM2’s memory mechanism for multi-frame processing, which may be less effective for single-image segmentation compared to VideoLISA’s single-token approach.

Table 3. Performance comparison with previous methods on referring and reasoning image segmentation datasets.

Method	Backbone	refCOCO			refCOCO+			refCOCOg		ReaSeg (val)		ReaSeg (test)	
		val	testA	testB	val	testA	testB	val	test	gIoU	cIoU	gIoU	cIoU
CRIS [32]	ResNet101	70.5	73.2	66.1	62.3	68.1	53.7	59.9	60.4	-	-	-	-
LAVT [41]	Swin-B	72.7	75.8	68.8	62.1	68.4	55.1	61.2	62.1	-	-	-	-
ReLA [18]	Swin-B	73.8	76.5	70.2	66.0	71.0	57.7	65.0	66.0	-	-	-	-
X-Decoder [46]	DaViT-L	-	-	-	-	-	-	64.6	-	22.6	17.9	21.7	16.3
SEEM [47]	DaViT-L	-	-	-	-	-	-	65.7	-	25.5	21.2	24.3	18.7
LISA [15]	LLaVA-7B	74.9	79.1	72.3	65.1	70.8	58.1	67.9	70.6	52.9	54.0	47.3	48.4
VISA [37]	Chat-UniVi-7B	72.4	75.5	68.1	59.8	64.8	53.1	65.5	66.4	52.7	57.8	-	-
VideoLISA [1]	LLaVA-Phi-3-V	73.8	76.6	68.8	63.4	68.8	56.2	68.3	68.8	61.4	67.1	53.8	54.4
VRS-HQ	Chat-UniVi-7B	73.5	77.5	69.5	61.7	67.6	54.3	66.7	67.5	55.2	51.8	51.7	52.9

Table 4. Ablation analysis of the fusion coefficient α .

α	referring			reasoning		
	\mathcal{J}	\mathcal{F}	$\mathcal{J}\&\mathcal{F}$	\mathcal{J}	\mathcal{F}	$\mathcal{J}\&\mathcal{F}$
0	56.5	61.1	58.8	51.5	56.7	54.1
0.1	59.8	64.5	62.1	53.5	58.7	56.1
0.25	58.9	63.8	61.3	52.3	57.8	55.0
0.5	58.2	63.0	60.6	51.4	56.6	54.0

Table 5. Ablation analysis of Token-driven Keyframe Selection. S_1 , S_2 , and S_3 represent CLIP scores, token similarity scores, and occlusion scores, respectively.

S_1	S_2	S_3	referring			reasoning		
			\mathcal{J}	\mathcal{F}	$\mathcal{J}\&\mathcal{F}$	\mathcal{J}	\mathcal{F}	$\mathcal{J}\&\mathcal{F}$
✓	✓	✓	59.7	64.2	61.9	52.5	57.8	55.2
✓	✓		57.8	62.4	60.1	50.9	56.2	53.6
✓		✓	59.6	64.1	61.8	52.5	57.7	55.1
	✓	✓	59.8	64.5	62.1	53.5	58.7	56.1

4.4. Ablation Studies

Fusion Coefficient Ablation. The ablation analysis of the fusion coefficient α in the TDA is illustrated in Tab. 4. An α of 0.1 yields optimal performance. Setting α to 0 leads to a sharp drop in the model’s performance as $\langle \text{TAK} \rangle$ fails to capture fine-grained intra-frame details, and the $\langle \text{SEG} \rangle$ token cannot be jointly optimized with $\langle \text{TAK} \rangle$ through backpropagation (e.g., **62.1%** \rightarrow **58.8%** $\mathcal{J}\&\mathcal{F}$ on the referring subset, **56.1%** \rightarrow **54.1%** $\mathcal{J}\&\mathcal{F}$ on the reasoning subset). As α increases beyond 0.1, the metrics decline slightly, likely due to excessive frame-level noise being introduced into the temporal token at a higher fusion coefficient (e.g., **62.1%** \rightarrow **60.6%** $\mathcal{J}\&\mathcal{F}$ on the referring subset, **56.1%** \rightarrow **54.0%** $\mathcal{J}\&\mathcal{F}$ on the reasoning subset).

Token-driven Keyframe Selection. Tab. 5 analyzes the impact of different score combinations for keyframe selection within the TKS. Results indicate that the occlusion score is the most influential of the three considered, improving $\mathcal{J}\&\mathcal{F}$ by **1.8%** and **1.6%** on the referring and reasoning subsets, respectively (first two rows). This improvement stems from the occlusion score’s ability to reflect the target object’s presence within each frame. The model achieves its best performance when keyframe selection is

Table 6. Ablation analysis of the mask decoding and propagation strategy. MT/MI: Multi-frame Training/Inference. ST/SI: Single-frame Training/Inference.

Strategy	referring			reasoning		
	\mathcal{J}	\mathcal{F}	$\mathcal{J}\&\mathcal{F}$	\mathcal{J}	\mathcal{F}	$\mathcal{J}\&\mathcal{F}$
SAM+ST+SI	48.3	52.4	50.3	42.9	47.4	45.2
SAM2+ST+SI	55.9	59.8	57.8	49.3	54.0	51.6
SAM2+ST+MI	55.8	60.8	58.3	46.5	52.5	49.5
SAM2+MT+SI	54.1	57.4	55.8	48.2	52.2	50.2
SAM2+MT+MI	59.8	64.5	62.1	53.5	58.7	56.1

Table 7. Ablation analysis of sampling strategy.

Sampling strategy	referring			reasoning		
	\mathcal{J}	\mathcal{F}	$\mathcal{J}\&\mathcal{F}$	\mathcal{J}	\mathcal{F}	$\mathcal{J}\&\mathcal{F}$
Random Sampling	59.0	63.6	61.3	53.2	58.4	55.8
Uniform Sampling	59.3	63.9	61.6	53.3	58.4	55.8
CLIP Sampling	59.8	64.5	62.1	53.5	58.7	56.1

based on a combination of token similarity and the occlusion score. However, incorporating the CLIP score (rows 1 and 4) slightly degrades performance (by **0.2%** and **0.9%** $\mathcal{J}\&\mathcal{F}$ on the referring and reasoning subsets, respectively), likely due to CLIP’s limited spatiotemporal understanding, which hinders accurate keyframe selection.

Mask Decoding and Propagation. Tab. 6 analyzes the impact of different mask decoding and propagation strategies on segmentation performance. Using only SAM and TDA for single-frame segmentation (first row) already surpasses VISA-13B by **0.9%**/**0.7%**/**0.9%** on the reasoning subset. Comparing the first two rows reveals the substantial advantage of SAM2 over SAM for single-frame fine-tuning and inference. SAM2 achieves improvements of **7.6%**/**7.4%**/**7.5%**/**6.4%**/**6.6%**/**6.4%**, demonstrating its superior robustness in segmentation and tracking. Furthermore, incorporating multi-frame propagation during both training and inference (last row) yields the best overall results, effectively leveraging SAM2’s memory mechanism for keyframe mask storage. This approach leads to further improvements in $\mathcal{J}\&\mathcal{F}$ of **3.8%** and **4.5%** compared to the other strategies.

Inference-Time Sampling Strategy. Tab. 7 analyzes the impact of different frame sampling strategies during inference. “Random” denotes randomly selected frames, while

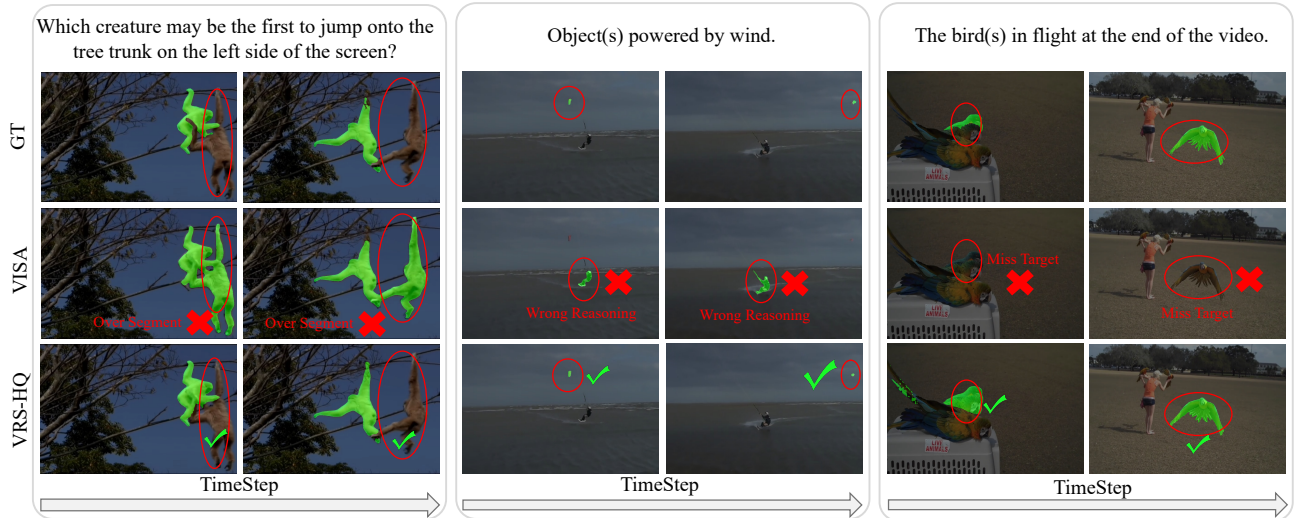


Figure 3. Segmentation map comparison of VISA and VRS-HQ on the ReVOS benchmark (§4.5). Results across three scenarios demonstrate that VRS-HQ excels in reasoning complex spatial and temporal relationships, delivering enhanced segmentation performance.

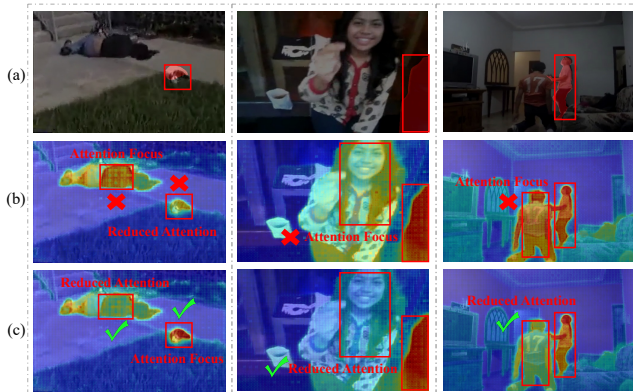


Figure 4. Visualization of feature maps (§4.5). From top to bottom are: (a) Ground truth masks. (b) Keyframe mask embeddings generated by the $\langle \text{TAK} \rangle$ token *before* TDA. (c) Keyframe mask embeddings generated by the $\langle \text{TAK} \rangle$ token *after* TDA.

“Uniform” extracts frames at equal intervals. CLIP sampling slightly outperforms uniform sampling, improving $\mathcal{J} \& \mathcal{F}$ by **0.5%/0.3%** on the referring and reasoning subsets, respectively. This modest gain is likely due to CLIP’s ability in selecting frames that are semantically aligned with the referring expression, which in turn facilitates the reasoning process of the MLLM.

4.5. Visualization Analysis

Segmentation Map Comparison. Fig. 3 presents the qualitative comparison of VRS-HQ and VISA on the ReVOS dataset across three different scenarios. In the left case, VISA displays ambiguity in spatial positioning and neglects critical references such as “the first”, revealing its limited semantic understanding. In contrast, VRS-HQ demonstrates a strong ability to perceive spatiotemporal re-

lationships. For the middle example, VISA mistakenly segments the person flying the kite, while VRS-HQ correctly identifies the kite, reflecting the stronger capacity to apply world knowledge and better handling of small-object segmentation. The right column showcases VRS-HQ’s robust temporal reasoning capabilities, driven by our temporal dynamic aggregation and adaptive keyframe selection. Conversely, VISA misses the target due to incorrect keyframe selection during inference.

Feature Visualization. To understand the TDA’s impact, we visualize mask embeddings generated by the mask decoder using both the fused and unfused $\langle \text{TAK} \rangle$ tokens with keyframe features. As illustrated in Fig. 4, we employ Principal Component Analysis (PCA) [33] to reduce the dimensionality of the mask embeddings to a single channel. This single-channel representation is then blended with the original image to highlight high-attention regions. Before TDA fusion, the $\langle \text{TAK} \rangle$ token often focuses on non-target elements (e.g., the falling person in the first example, the woman in the second, and the central dancing man in the third). In contrast, the similarity-weighted fusion of the frame-level SEG tokens into the $\langle \text{TAK} \rangle$ token significantly enriches the positional and semantic information contained within the token, enabling the model to more effectively concentrate on the correlated target objects.

5. Conclusion

We present VRS-HQ, a novel approach that leverages the temporal reasoning of MLLM and the robust tracking of SAM2 for high-quality Video Reasoning Segmentation. Our method utilizes a temporal-level $\langle \text{TAK} \rangle$ token and frame-level $\langle \text{SEG} \rangle$ tokens to capture temporal relations and spatial features, respectively. These tokens are integrated

using the Temporal Dynamic Aggregation, with SAM2 utilizing the $\langle \text{TAK} \rangle$ token for keyframe segmentation and mask propagation. Moreover, we introduce a Token-driven Keyframe Selection that uses the $\langle \text{TAK} \rangle$ token to generate occlusion scores for robust keyframe selection. Extensive experiments confirm that VRS-HQ achieves state-of-the-art performance on various benchmarks, demonstrating strong capabilities in handling Video Reasoning Segmentation.

6. Appendix

This supplementary material provides additional details and analysis of VRS-HQ, expanding on the content presented in the main paper. We begin by evaluating the impact of various training datasets on segmentation performance (§A). Next, we present more detailed implementation information to facilitate reproducibility (§B). We then elaborate on the specific method of utilizing SAM2 [27] for mask decoding and propagation (§C). Subsequently, we show some failure cases with analysis to offer a more comprehensive understanding of VRS-HQ’s limitations (§D). Additionally, we present more qualitative comparisons against VISA, highlighting the strengths of our proposed method (§E). Finally, we visualize the reasoning segmentation results of VRS-HQ on in-the-wild video datasets, demonstrating its strong generalization capabilities (§F).

A. Datasets Ablation

As illustrated in Tab. 8, fine-tuning with the full datasets yields the best performance while excluding the image segmentation dataset, VideoQA dataset [20], or ReVOS dataset [37] individually results in varying degrees of metric degradation. Notably, removing the VideoQA dataset minimally impacts the model’s performance, with a decline of **0.9%** in $\mathcal{J} \& \mathcal{F}$ on both the referring and reasoning subsets, as its primary role is to support the MLLM’s video comprehension rather than directly contributing to the segmentation process. In contrast, excluding the ReVOS dataset leads to a noticeable drop of **4.4%** and **7.6%** in $\mathcal{J} \& \mathcal{F}$, highlighting its pivotal role in enhancing the model’s reasoning segmentation performance in challenging scenarios.

Table 8. Ablation study on the impact of training datasets.

Datasets	referring			reasoning		
	\mathcal{J}	\mathcal{F}	$\mathcal{J} \& \mathcal{F}$	\mathcal{J}	\mathcal{F}	$\mathcal{J} \& \mathcal{F}$
Joint	59.8	64.5	62.1	53.5	58.7	56.1
w/o ImageSeg	58.5	63.2	60.8	51.0	56.3	53.6
w/o VideoQA	<u>58.7</u>	<u>63.7</u>	<u>61.2</u>	<u>52.4</u>	<u>58.0</u>	<u>55.2</u>
w/o ReVOS	55.3	60.1	57.7	45.3	51.6	48.5

B. Additional Implementation Details

Due to space constraints of the main document, additional implementation details are provided here. During train-

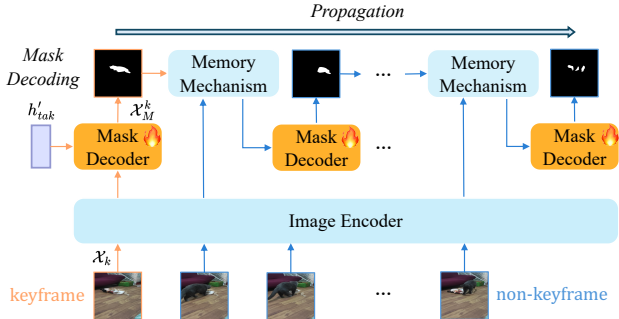


Figure 5. Details of SAM2 for mask decoding and propagation. All the video frames are input into the image encoder for feature extraction. The feature embeddings of the keyframe interact with h_{tak}^k through the mask decoder for mask generation and then propagate it to the remaining video frames via the memory mechanism.

ing, we use varying sampling ratios for different datasets (cf. Tab. 9). For video segmentation datasets, 8-12 frames are uniformly sampled at fixed intervals per video, and up to three object categories are selected per image or video. During inference, we utilize CLIP-336 [23] for global sampling, selecting up to 12 frames per video. Input images are resized to 224×224 before being input to Chat-UniVi [12]. Data passed to SAM2 is augmented as described in [14] and resized to 1024×1024 . Moreover, LoRA [10] is applied with a scaling factor of 16 and a dropout rate of 0.05 across all query and value projection layers within the MLLM, enabling efficient fine-tuning.

Table 9. Datasets sampling ratio during training.

Dataset	SemSeg	RIS	ImageQA	ReaSeg	VideoQA	VideoSeg
Ratios	9/32	3/32	3/32	1/32	1/8	3/8

C. More Details of SAM2

As depicted in Fig. 5, we provide detailed insights into the process of mask decoding and propagation using SAM2 [27]. Specifically, all input video frames are processed through the image encoder to extract multi-scale visual features. Subsequently, the fused temporal embedding h_{tak}^k interacts with the keyframe features in the mask decoder to generate the segmentation mask and perform video-level propagation. The prediction is then encoded by the memory encoder and stored in the memory bank, which maintains a FIFO queue of memories from recent frames. Feature embeddings from subsequent non-keyframes attend to these stored mask features through memory attention and utilize the mask decoder to generate corresponding masks, enabling inter-frame propagation.

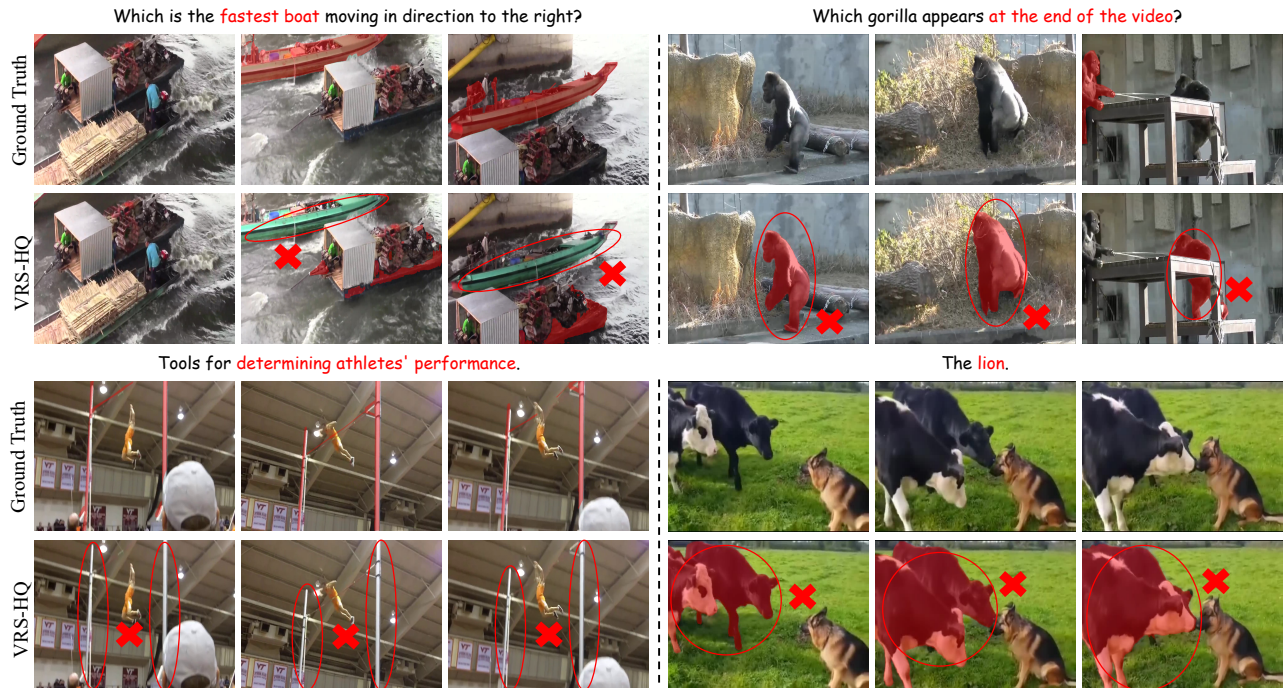


Figure 6. Visualization of failure cases for VRS-HQ. These examples illustrate the model’s limitations in scenarios requiring complex world knowledge and temporal reasoning, as well as challenges in processing negative samples.

D. Failure Case Analysis

Fig. 6 presents a detailed analysis of several failure cases, offering a deeper understanding of the limitations of VRS-HQ. The **top row** highlights two specific challenges. **First**, VRS-HQ struggles with keyframe localization when presented with queries based on motion, such as identifying the fastest-moving boat within a video sequence. This suggests a potential weakness in analyzing and interpreting dynamic visual information. **Second**, the model exhibits difficulty segmenting targets with minimal temporal presence, as exemplified by the gorilla visible only in the last two frames of the video. This points to a possible limitation in effectively capturing and utilizing short-duration visual cues. The **bottom row** reveals further limitations. VRS-HQ demonstrates a lack of comprehension when faced with nuanced or implicitly phrased prompts, such as recognizing a “high bar” within the context of gymnastics performance evaluation. This suggests a need for improved understanding of complex semantic relationships within video content. Furthermore, the model occasionally exhibits hallucinatory behavior, generating segmentations for non-existent objects, particularly when dealing with empty targets or scenes where the requested object is absent.

We hypothesize that several strategies could mitigate these limitations. Improving the video comprehension capabilities of the Multimodal Large Language Model

(MLLM) could enhance the ability to interpret complex scenes and queries. Enabling the model to process a larger number of sampled frames simultaneously might improve its sensitivity to subtle temporal changes and short-duration events. Finally, designing specialized tokens specifically for representing empty masks could address the observed hallucinations in such scenarios. We leave a thorough investigation of these potential improvements to future research.

E. More Qualitative Comparison

In addition to the visual comparisons presented in the main document, we provide further comparisons across more diverse settings in Fig. 7-9 to demonstrate the model’s reasoning and segmentation capabilities. As illustrated in Fig. 7, VISA demonstrates reduced sensitivity to color-related expressions (e.g., “white” and “brown”) when provided with explicit textual instructions. Furthermore, the example on the left demonstrates VISA’s tendency to misidentify visually similar objects with complex spatial variations. In contrast, VRS-HQ effectively aggregates temporal information, capturing inter-frame motion dynamics and leading to improved segmentation accuracy.

Fig. 8 highlights the robust segmentation and reasoning capabilities of VRS-HQ in scenarios with complex temporal dynamics. In the left example, VISA struggles to precisely detect the airplane appearing on the left at the end of the video. Similarly, in the right case, VISA misclas-

sifies the tiger emerging in the lower left corner. In contrast, VRS-HQ leverages the Token-driven Keyframe Selection for more accurate keyframe identification and integrates SAM2 with the temporal token, enriched with both intra-frame spatial and inter-frame temporal relations, resulting in reliable decoding and consistent object tracking.

Fig. 9 presents scenarios requiring general and world knowledge for reasoning. In the first example (left), VISA segments only two koi carp (*Cyprinus carpio*) correctly, whereas VRS-HQ identifies nearly all the fish present. In the second example (right), VISA fails to associate “dog” with the phrase “common household pet”, indicating limitations in its reasoning capabilities. By contrast, VRS-HQ leverages the integration of temporal tokens to achieve a more nuanced semantic understanding, enabling finer control and interpretation.

F. In-the-wild Visualization Results

Fig. 10 and Fig. 11 show qualitative results of VRS-HQ on in-the-wild videos. Fig. 10 shows results on first-person videos from the GTEA dataset [8], using implicit prompts. Even in cluttered kitchen environments with many similar objects, VRS-HQ demonstrates strong generalization capability. It is particularly effective at segmenting smaller targets, such as the spoon and watch shown in the first and third rows, respectively, maintaining robust performance in these challenging scenarios. Fig. 11 shows results on 360-degree panoramic videos from the PanoVOS dataset [39], using more intricate prompts. Notably, VRS-HQ successfully segments individuals even when they are split across the distorted edges of the video (first row), without any task-specific optimizations. Furthermore, it maintains effective tracking performance when the primary subjects within the video are moving dynamically (last two rows).

References

- [1] Zechen Bai, Tong He, Haiyang Mei, Pichao Wang, Ziteng Gao, Joya Chen, Lei Liu, Zheng Zhang, and Mike Zheng Shou. One token to seg them all: Language instructed reasoning segmentation in videos. In *Adv. Neural Inform. Process. Syst.*, 2024. 1, 4, 5, 6, 7
- [2] Adam Botach, Evgenii Zheltonozhskii, and Chaim Baskin. End-to-end referring video object segmentation with multimodal transformers. In *IEEE Conf. Comput. Vis. Pattern Recog.*, pages 4985–4995, 2022. 2, 3, 5, 6
- [3] Holger Caesar, Jasper Uijlings, and Vittorio Ferrari. Coco-stuff: Thing and stuff classes in context. In *IEEE Conf. Comput. Vis. Pattern Recog.*, pages 1209–1218, 2018. 5
- [4] Nicolas Carion, Francisco Massa, Gabriel Synnaeve, Nicolas Usunier, Alexander Kirillov, and Sergey Zagoruyko. End-to-end object detection with transformers. In *Eur. Conf. Comput. Vis.*, pages 213–229. Springer, 2020. 3
- [5] Xianjie Chen, Roozbeh Mottaghi, Xiaobai Liu, Sanja Fidler, Raquel Urtasun, and Alan Yuille. Detect what you can: Detecting and representing objects using holistic models and body parts. In *IEEE Conf. Comput. Vis. Pattern Recog.*, pages 1971–1978, 2014. 5
- [6] Ho Kei Cheng and Alexander G Schwing. Xmem: Long-term video object segmentation with an atkinson-shiffrin memory model. In *Eur. Conf. Comput. Vis.*, pages 640–658. Springer, 2022. 1
- [7] Henghui Ding, Chang Liu, Shuting He, Xudong Jiang, and Chen Change Loy. Mevis: A large-scale benchmark for video segmentation with motion expressions. In *Int. Conf. Comput. Vis.*, pages 2694–2703, 2023. 5, 6
- [8] Alireza Fathi, Xiaofeng Ren, and James M Rehg. Learning to recognize objects in egocentric activities. In *CVPR 2011*, pages 3281–3288. IEEE, 2011. 11
- [9] Junwen He, Yifan Wang, Lijun Wang, Huchuan Lu, Jun-Yan He, Jin-Peng Lan, Bin Luo, and Xuansong Xie. Multi-modal instruction tuned llms with fine-grained visual perception. In *IEEE Conf. Comput. Vis. Pattern Recog.*, pages 13980–13990, 2024. 1
- [10] Edward J Hu, Yelong Shen, Phillip Wallis, Zeyuan Allen-Zhu, Yuanzhi Li, Shean Wang, Lu Wang, and Weizhu Chen. Lora: Low-rank adaptation of large language models. *arXiv preprint arXiv:2106.09685*, 2021. 5, 9
- [11] Tianrui Hui, Shaofei Huang, Si Liu, Zihan Ding, Guanbin Li, Wenguan Wang, Jizhong Han, and Fei Wang. Collaborative spatial-temporal modeling for language-queried video actor segmentation. In *IEEE Conf. Comput. Vis. Pattern Recog.*, pages 4187–4196, 2021. 3
- [12] Peng Jin, Ryuichi Takanobu, Wancai Zhang, Xiaochun Cao, and Li Yuan. Chat-univi: Unified visual representation empowers large language models with image and video understanding. In *IEEE Conf. Comput. Vis. Pattern Recog.*, pages 13700–13710, 2024. 4, 5, 9
- [13] Sahar Kazemzadeh, Vicente Ordonez, Mark Matten, and Tamara Berg. Referitgame: Referring to objects in photographs of natural scenes. In *Proceedings of the 2014 conference on empirical methods in natural language processing (EMNLP)*, pages 787–798, 2014. 5
- [14] Alexander Kirillov, Eric Mintun, Nikhila Ravi, Hanzi Mao, Chloe Rolland, Laura Gustafson, Tete Xiao, Spencer Whitehead, Alexander C Berg, Wan-Yen Lo, et al. Segment anything. In *Int. Conf. Comput. Vis.*, pages 4015–4026, 2023. 1, 9

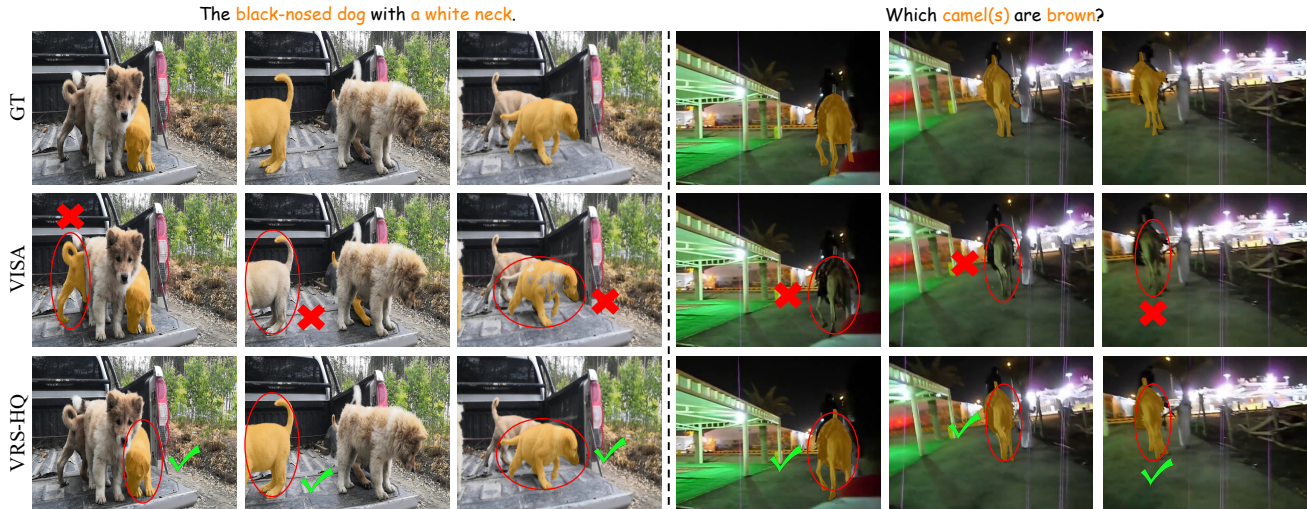


Figure 7. Qualitative comparison of VRS-HQ and VISA in explicit language-based referring scenarios on the ReVOS benchmark.

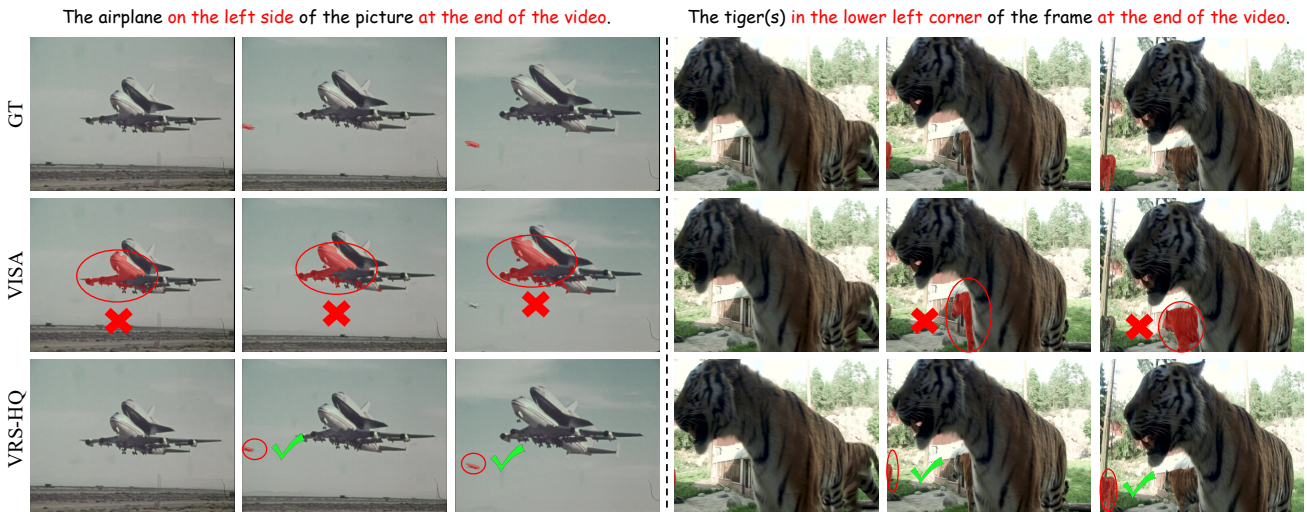


Figure 8. Qualitative comparison of VRS-HQ and VISA in scenarios incorporating complex temporal dynamics on the ReVOS benchmark.

- [15] Xin Lai, Zhuotao Tian, Yukang Chen, Yanwei Li, Yuhui Yuan, Shu Liu, and Jiaya Jia. Lisa: Reasoning segmentation via large language model. In *IEEE Conf. Comput. Vis. Pattern Recog.*, pages 9579–9589, 2024. [1](#), [3](#), [5](#), [6](#), [7](#)
- [16] Junnan Li, Dongxu Li, Silvio Savarese, and Steven Hoi. Blip-2: Bootstrapping language-image pre-training with frozen image encoders and large language models. In *Int. Conf. Mach. Learn.*, pages 19730–19742. PMLR, 2023. [1](#)
- [17] Yanwei Li, Chengyao Wang, and Jiaya Jia. Llama-vid: An image is worth 2 tokens in large language models. In *Eur. Conf. Comput. Vis.*, pages 323–340. Springer, 2025. [1](#), [4](#), [6](#)
- [18] Chang Liu, Henghui Ding, and Xudong Jiang. Gres: Generalized referring expression segmentation. In *IEEE Conf. Comput. Vis. Pattern Recog.*, pages 23592–23601, 2023. [7](#)
- [19] Haotian Liu, Chunyuan Li, Qingyang Wu, and Yong Jae Lee. Visual instruction tuning. *Adv. Neural Inform. Process. Syst.*, 36, 2024. [1](#), [5](#)
- [20] Muhammad Maaz, Hanoona Rasheed, Salman Khan, and Fahad Shahbaz Khan. Video-chatgpt: Towards detailed video understanding via large vision and language models. *arXiv preprint arXiv:2306.05424*, 2023. [5](#), [9](#)
- [21] Junhua Mao, Jonathan Huang, Alexander Toshev, Oana Camburu, Alan L Yuille, and Kevin Murphy. Generation and comprehension of unambiguous object descriptions. In *CVPR*, pages 11–20, 2016. [5](#)
- [22] Jordi Pont-Tuset, Federico Perazzi, Sergi Caelles, Pablo Arbeláez, Alex Sorkine-Hornung, and Luc

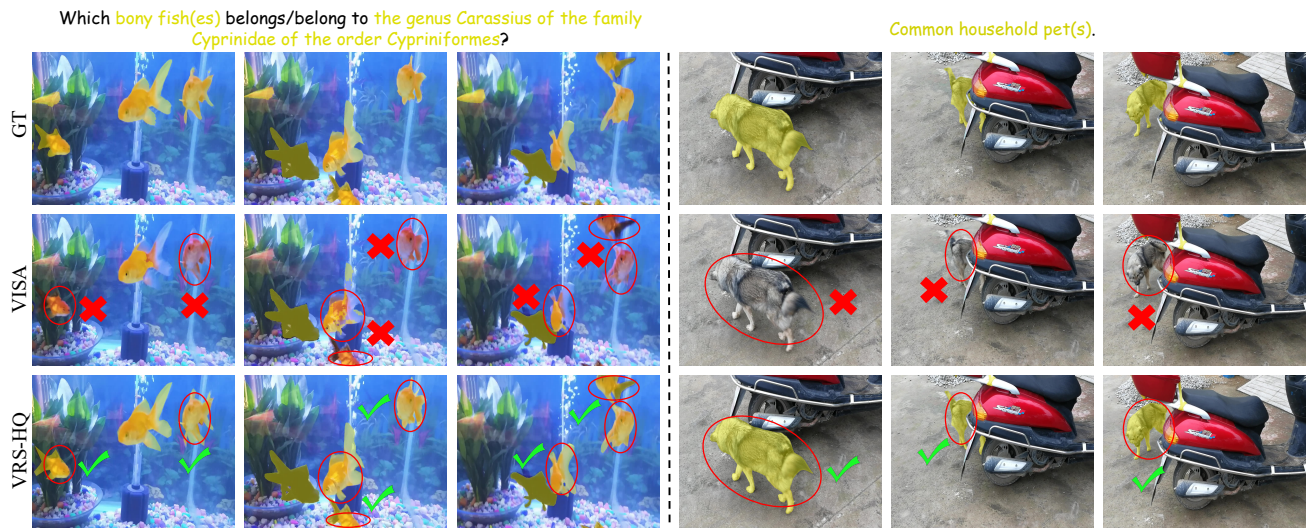


Figure 9. Qualitative comparison of VRS-HQ and VISA in reasoning scenarios that require world knowledge on the ReVOS benchmark. The video's subject uses a curved tool for scooping and serving liquids or soft solids, which typically features a rounded bowl and a handle, ensuring ease of use and practicality.

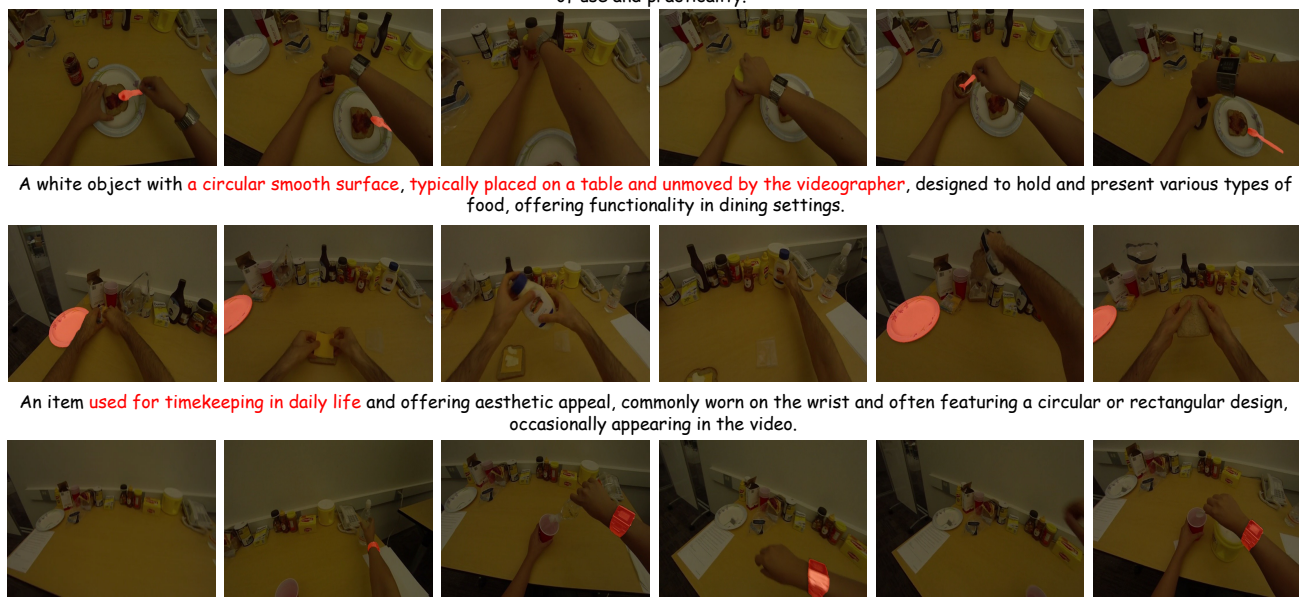


Figure 10. Visualization of VRS-HQ utilized in egocentric videos.

Van Gool. The 2017 davis challenge on video object segmentation. *arXiv preprint arXiv:1704.00675*, 2017. 5

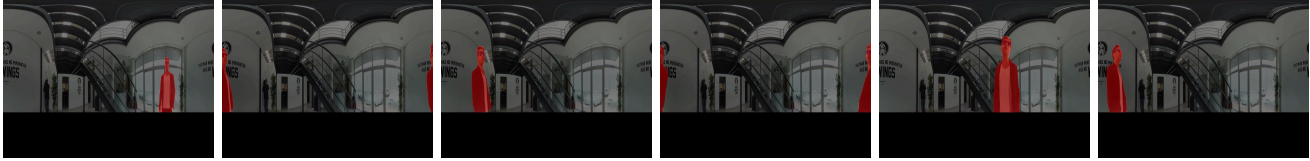
[23] Alec Radford, Jong Wook Kim, Chris Hallacy, Aditya Ramesh, Gabriel Goh, Sandhini Agarwal, Girish Sastry, Amanda Askell, Pamela Mishkin, Jack Clark, et al. Learning transferable visual models from natural language supervision. In *Int. Conf. Mach. Learn.*, pages 8748–8763. PMLR, 2021. 4, 9

[24] Vignesh Ramanathan, Anmol Kalia, Vladan Petrovic, Yi Wen, Baixue Zheng, Baishan Guo, Rui Wang, Aaron Marquez, Rama Kovvuri, Abhishek Kadian, et al. Paco: Parts and attributes of common objects. In *IEEE Conf. Comput. Vis. Pattern Recog.*, pages 7141–7151, 2023. 5

[25] Hanoona Rasheed, Muhammad Maaz, Sahal Shaji, Abdelrahman Shaker, Salman Khan, Hisham Cholakkal, Rao M Anwer, Eric Xing, Ming-Hsuan Yang, and Fahad S Khan. Glamm: Pixel grounding large multimodal model. In *IEEE Conf. Comput. Vis. Pattern Recog.*, pages 13009–13018, 2024. 1, 3

[26] Jeff Rasley, Samyam Rajbhandari, Olatunji Ruwase, and Yuxiong He. Deepspeed: System optimizations enable training deep learning models with over 100 billion parameters. In *Proc. ACM SIGKDD Int. Conf. Knowl. Discov. Data Min.*, pages 3505–3506, 2020. 5

A prominent figure subtly highlighted within a commercial promotional video, whose presence and actions serve as the central point for engagement and communication.



The individual demonstrating a more seasoned presence and refined mastery of BMX Freestyle maneuvers, embodying the skill and experience often associated with years of dedication to the sport.



Who displays the most dynamic and expressive range of movement during the dance, transitioning seamlessly between sharp, high-energy motions, captivating attention with their vibrant and energetic performance.



Figure 11. Visualization of VRS-HQ applied to 360-degree panoramic videos.

- [27] Nikhila Ravi, Valentin Gabeur, Yuan-Ting Hu, Ronghang Hu, Chaitanya Ryali, Tengyu Ma, Haitham Khedr, Roman Rädle, Chloe Rolland, Laura Gustafson, et al. Sam 2: Segment anything in images and videos. *arXiv preprint arXiv:2408.00714*, 2024. [1](#), [9](#)
- [28] Zhongwei Ren, Zhicheng Huang, Yunchao Wei, Yao Zhao, Dongmei Fu, Jiashi Feng, and Xiaojie Jin. Pixellm: Pixel reasoning with large multimodal model. In *IEEE Conf. Comput. Vis. Pattern Recog.*, pages 26374–26383, 2024. [1](#), [3](#)
- [29] Hamid Rezaatofghi, Nathan Tsoi, JunYoung Gwak, Amir Sadeghian, Ian Reid, and Silvio Savarese. Generalized intersection over union: A metric and a loss for bounding box regression. In *Proceedings of the IEEE/CVF conference on computer vision and pattern recognition*, pages 658–666, 2019. [5](#)
- [30] Seonguk Seo, Joon-Young Lee, and Bohyung Han. Urvos: Unified referring video object segmentation network with a large-scale benchmark. In *Eur. Conf. Comput. Vis.*, pages 208–223. Springer, 2020. [3](#), [5](#)
- [31] Hao Wang, Cheng Deng, Junchi Yan, and Dacheng Tao. Asymmetric cross-guided attention network for actor and action video segmentation from natural language query. In *Int. Conf. Comput. Vis.*, pages 3939–3948, 2019. [2](#)
- [32] Zhaoqing Wang, Yu Lu, Qiang Li, Xunqiang Tao, Yandong Guo, Mingming Gong, and Tongliang Liu. Cris: Clip-driven referring image segmentation. In *IEEE Conf. Comput. Vis. Pattern Recog.*, pages 11686–11695, 2022. [7](#)
- [33] Svante Wold, Kim Esbensen, and Paul Geladi. Principal component analysis. *Chemometrics and intelligent laboratory systems*, 2(1-3):37–52, 1987. [8](#)
- [34] Dongming Wu, Tiancai Wang, Yuang Zhang, Xiangyu Zhang, and Jianbing Shen. Onlinerefer: A simple online baseline for referring video object segmentation. In *Int. Conf. Comput. Vis.*, pages 2761–2770, 2023. [1](#), [6](#)
- [35] Jiannan Wu, Yi Jiang, Peize Sun, Zehuan Yuan, and Ping Luo. Language as queries for referring video object segmentation. In *IEEE Conf. Comput. Vis. Pattern Recog.*, pages 4974–4984, 2022. [1](#), [2](#), [3](#), [5](#), [6](#)
- [36] Zhuofan Xia, Dongchen Han, Yizeng Han, Xuran Pan, Shiji Song, and Gao Huang. Gsva: Generalized segmentation via multimodal large language models. In *IEEE Conf. Comput. Vis. Pattern Recog.*, pages 3858–3869, 2024. [1](#), [3](#)
- [37] Cilin Yan, Haochen Wang, Shilin Yan, Xiaolong Jiang, Yao Hu, Guoliang Kang, Weidi Xie, and Efstratios Gavves. Visa: Reasoning video object segmentation via large language models. In *Eur. Conf. Comput. Vis.*, 2024. [1](#), [2](#), [3](#), [4](#), [5](#), [6](#), [7](#), [9](#)
- [38] Shilin Yan, Renrui Zhang, Ziyu Guo, Wenchao Chen, Wei Zhang, Hongyang Li, Yu Qiao, Hao Dong, Zhongjiang He, and Peng Gao. Referred by multimodality: A unified temporal transformer for video object segmentation. In *AAAI*, pages 6449–6457, 2024. [1](#), [2](#)
- [39] Shilin Yan, Xiaohao Xu, Renrui Zhang, Lingyi Hong, Wenchao Chen, Wenqiang Zhang, and Wei Zhang. Panovos: Bridging non-panoramic and panoramic

- views with transformer for video segmentation. In *European Conference on Computer Vision*, pages 346–365. Springer, 2025. 11
- [40] Senqiao Yang, Tianyuan Qu, Xin Lai, Zhuotao Tian, Bohao Peng, Shu Liu, and Jiaya Jia. An improved baseline for reasoning segmentation with large language model. *arXiv e-prints*, pages arXiv–2312, 2023. 3
- [41] Zhao Yang, Jiaqi Wang, Yansong Tang, Kai Chen, Hengshuang Zhao, and Philip HS Torr. Lavt: Language-aware vision transformer for referring image segmentation. In *IEEE Conf. Comput. Vis. Pattern Recog.*, pages 18155–18165, 2022. 7
- [42] Rongkun Zheng, Lu Qi, Xi Chen, Yi Wang, Kun Wang, Yu Qiao, and Hengshuang Zhao. Villa: Video reasoning segmentation with large language model. *arXiv preprint arXiv:2407.14500*, 2024. 1, 5
- [43] Zhaohui Zheng, Ping Wang, Wei Liu, Jinze Li, Rongguang Ye, and Dongwei Ren. Distance-iou loss: Faster and better learning for bounding box regression. In *AAAI*, pages 12993–13000, 2020. 5
- [44] Bolei Zhou, Hang Zhao, Xavier Puig, Sanja Fidler, Adela Barriuso, and Antonio Torralba. Scene parsing through ade20k dataset. In *CVPR*, pages 633–641, 2017. 5
- [45] Jiawen Zhu, Zhi-Qi Cheng, Jun-Yan He, Chenyang Li, Bin Luo, Huchuan Lu, Yifeng Geng, and Xuansong Xie. Tracking with human-intent reasoning. *arXiv preprint arXiv:2312.17448*, 2023. 5, 6
- [46] Xueyan Zou, Zi-Yi Dou, Jianwei Yang, Zhe Gan, Linjie Li, Chunyuan Li, Xiyang Dai, Harkirat Behl, Jianfeng Wang, Lu Yuan, et al. Generalized decoding for pixel, image, and language. In *IEEE Conf. Comput. Vis. Pattern Recog.*, pages 15116–15127, 2023. 7
- [47] Xueyan Zou, Jianwei Yang, Hao Zhang, Feng Li, Linjie Li, Jianfeng Wang, Lijuan Wang, Jianfeng Gao, and Yong Jae Lee. Segment everything everywhere all at once. *Adv. Neural Inform. Process. Syst.*, 36, 2024. 7